Dissolved Oxygen Redox as the Source of Hydrogen Peroxide and Hydroxyl Radical in Sonicated Emulsive Water Microdroplets

Abdelilah Asserghine[1,2,‡], Aravind Baby[1,3,‡], Jeanne N'Diaye[1,2], Adolfo I. B. Romo[1], Supriya Das[1,2], Chloe A. Litts[1], Prashant K. Jain[1], Joaquín Rodríguez-López[1,2,*]

[1]Department of Chemistry, University of Illinois Urbana-Champaign, Urbana, IL 61801, USA

[2]Beckman Institute for Advanced Science and Technology, University of Illinois Urbana-Champaign, Urbana, IL 61801

[3]Department of Materials Science and Engineering, University of Illinois Urbana-Champaign, Urbana, IL 61801, USA.

‡These authors equally contributed

*To whom all correspondence should be addressed: E-mail: joaquinr@illinois.edu

KEYWORDS: Microdroplets, Redox, Oxygen, Hydrogen Peroxide, Hydroxyl Radical.

ABSTRACT: Sonicated emulsive water microdroplets (SEWMs) accelerate and enable a variety of catalyst-free chemical transformations. However, significant unanswered questions remain regarding the chemical intermediates they form and their possible redox origin. In this study, we identified dissolved O_2 as the primary originator of reactive oxygen species (ROS) such as $OH^•$ and H_2O_2. We uncovered the role of dissolved O_2 redox by using a combination of microelectrochemical methods to detect H_2O_2, isotopic methods to identify the source of H_2O_2, and a combination of electron spin resonance and the DMPO spin trap to detect radicals such as $OH^•$. Notably, we found that H_2O_2 production is correlated with O_2 content via a reduction pathway enabled by a sufficiently large reducing power that can additionally generate H_2 and even perform Pb electroless deposition on Au and Cu metal substrates. Building on our findings, continuous O_2 bubbling of SEWMs showed accumulation of H_2O_2 up to ~88 mM in the aqueous phase within one hour of sonication, demonstrating the scale-up promise of this method. Distinct to sonochemistry of a single phase, this study advances our understanding of the confluence of redox and chemical reaction mechanisms within SEWMs as a biphasic system. This insight paves the way for improving their reaction kinetics, yield, and selectivity, positioning these attractive redox microreactors as alternatives to traditional electrolyzers.

In recent years, water microdroplets have received significant attention as chemical microreactors that enable or accelerate a wide range of reactions, including redox transformations.[1-3] Microdroplet generation has been explored through versatile methods such as spray ionization, aerosols, and emulsions, and have been used in various applications, including catalysis, polymerization, and (electro)synthesis.[4-18] Despite these promising applications, the redox mechanisms underlying the formation of key intermediates within them, such as reactive oxygen species (ROS), are yet to be established.

In particular, redox reactions in sonicated emulsive water microdroplets (SEWMs) have been proposed to arise from oxidative chemistries facilitated by electric fields detected at the oil/water interface of microdroplets, as shown by using stimulated Raman excited fluorescence.[19] These measurements revealed a strong electric field of the order of 10^7 V/cm at a water-hexadecane oil interface.[19] Strong electric fields in SEWMs could help generate ROS like $OH^•$ and H_2O_2 by providing a driving force to spontaneously carry out redox transformation.[20] Recent studies have also suggested similar mechanisms in related droplet systems by detecting $OH^•$ and H_2O_2 in electrospray-ionized water microdroplets.[11,21-24] Most studies, however, suggest that ROS form via water homolysis (**reaction 1**), producing $OH^•$ and $H^•$, followed by $OH^•$ dimerizing to form H_2O_2 (**reaction 2**). Additionally, it has been suggested that redox in SEWMs is mediated by radicals, with $OH^•$ and $H^•$ acting as oxidizing and reducing agents, respectively.[19,25] However, in addition to H_2O as the source of ROS (**reactions 3-5**)[26] the oxidation of the oil at the interface could also contribute to redox.[27]

$$H_2O \rightleftharpoons OH^• + H^• \qquad \text{Reaction 1}$$

$$OH^• + OH^• \rightleftharpoons H_2O_2 \qquad \text{Reaction 2}$$

$$2H_2O \rightleftharpoons H_2O_2 + 2H^+ + 2e^- \qquad \text{Reaction 3}$$

$$H_2O \rightleftharpoons OH^• + H^+ + e^- \qquad \text{Reaction 4}$$

$$2H_2O \rightleftharpoons O_2 + 4H^+ + 4e^- \qquad \text{Reaction 5}$$

While **reactions 1-5** consider water oxidation as the source of ROS, our experience with the electrolysis of O_2 via the 2e oxygen reduction reaction (2e ORR, **reaction 6**) encouraged us to explore an alternative pathway based on exploring the overlooked reducing power of SEWMs. Such reducing power could result from transferrable electrons and/or $H^•$ prompted by interactions between the oil and water upon sonication, thus reducing dissolved O_2, and transforming H_2O_2 into $OH^•$ (**reaction 7**, or the reverse of **reaction 2**) within the SEWMs.

$$O_2 + 2H^+ + 2e^- \rightleftharpoons H_2O_2 \qquad \text{Reaction 6}$$

$$H_2O_2 + H^+ + e^- \rightleftharpoons H_2O + OH^• \qquad \text{Reaction 7}$$

To validate our proposal, we investigated the generation of H_2O_2, $OH^•$, and H_2 by SEWMs under different degrees of oxygenation, always in the absence of any catalyst. We employed a Pt-ultramicroelectrode (Pt-UME) to detect H_2O_2 and H_2, while employing radical trapping and electron spin resonance (ESR) spectroscopy to identify $OH^•$. We demonstrated that dissolved O_2 predominantly governs H_2O_2 production, with its excess leading to significant accumulations of H_2O_2. Additionally, we demonstrated electroless Pb^{2+} deposition on Au and Cu substrates using these SEWMs, suggesting that electron mediation is possible within them.

For generating SEWMs we used ultrasonication via a Bransonic M1800H ultrasonic bath with an output power of 70 W at a frequency of 40 kHz (Supplementary Note S1 discusses associated details). Immiscible mixtures of water and hexadecane oil in a 1:10 volume ratio were sonicated to form a transient emulsion for varying durations. Optical microscopy images of the sonicated systems showed a distribution of water microdroplet sizes from 1 to 20 μm (**Figure 1A**).

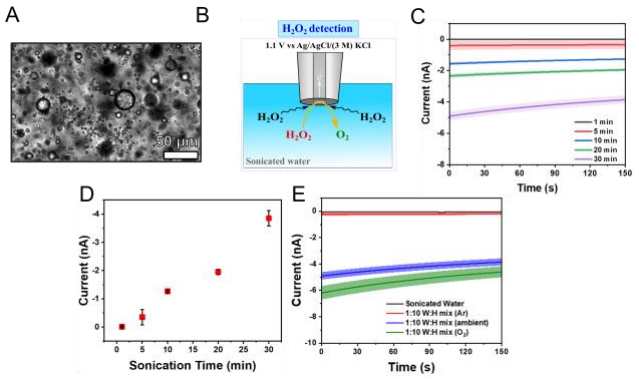

Figure 1: Electrochemical detection of H_2O_2 generated by SEWMs. (A) Optical image of the SEWMs. (B) Schematic representation of the experimental setup for H_2O_2 detection in the sonicated water phase, using a 12.5 μm Pt-UME biased at 1.1 V vs. Ag/AgCl (3M KCl). (C) Chronoamperogram showing H_2O_2 generation at various sonication times, with a 12.5 μm Pt-UME at 1.1 V vs. Ag/AgCl (3M KCl). (D) Kinetic analysis of H_2O_2 production across different sonication times. (E) Chronoamperograms obtained with a Pt-UME at 1.1 V vs. Ag/AgCl (3M KCl) under ambient, argon, and oxygen-saturated conditions. All the electrochemical measurements were performed with 0.1 M KNO_3 added after sonication (4x dilution).

First, under ambient conditions where the oil/water mixture was at equilibrium with the atmosphere, we detected the generation of H_2O_2 within SEWMs. H_2O_2 detection was carried out by employing a Pt-UME as an amperometric probe biased at 1.1 V vs Ag/AgCl/3 M KCl and placed in the sonicated water phase extracted by centrifugation (Supplementary Note S2), resulting in a steady state current as shown in **Figure 1B** and **1C**.[28] The recorded chronoamperograms in the extracted water phase show an oxidative current that increased with sonication time (**Figure 1C** and **1D**), exhibiting a fairly linear trend. The current measured at 30 min (-3.8 nA) corresponds to an estimated H_2O_2 concentration ≈ 8 mM in the extracted water phase (Figure S2D). The H_2O_2 was also confirmed through a positive iodometric test (Supplementary Note S3).

To validate our hypothesis that H_2O_2 is mediated through O_2 reduction within the SEWMs, we sonicated a 1:10 water-oil mixture for 30 minutes under both argon-saturated (de-oxygenated) and oxygen-saturated conditions (**Figure 1E**) and measured the resulting H_2O_2 current. Critically, we observed a significantly higher steady-state current in the presence of oxygen (-4.6 nA) compared to the negligible current under deaerated conditions (-0.2 nA), indicating that H_2O_2 generation strongly depends on the presence of O_2. This finding was also confirmed using isotope-labelling mass spectrometry measurements using 4-carboxyphenylboronic acid dissolved in $H_2{}^{18}O$ as a probe to investigate the source of H_2O_2 (Supplementary Note S4). The formation of the 4-carboxyphenol derivative, with an observed m/z of 139 in $H_2{}^{18}O$ compared to m/z of 137 expected for unlabelled water or environmental O_2 would indicate water as the source of H_2O_2 (**reactions 1-4**).[29] The mass spectra of the sonicated 1:1 $H_2{}^{18}O$-oil mixture in ambient conditions and in the presence of 1.5 mM 4-carboxyphenylboronic acid showed only the m/z peak at 137, indicating only the presence of unlabelled 4-carboxyphenol (Figure S7B and B). This confirms that H_2O_2 originates from O_2 reduction rather than $H_2{}^{18}O$ oxidation (**Figure S7 A)**. Additionally, the absence of the m/z peak at 137 under argon conditions (**Figure S7 B**) further supports that O_2 reduction is a critical reaction enhancing H_2O_2 generation within SEWMs during ultrasonication.

The mechanistic insight gained through the experiments above encouraged us to demonstrate the production of H_2O_2 at higher concentrations. Since H_2O_2 is water-miscible and non-volatile, we reasoned that continuously oxygenating a SEWM would allow H_2O_2 to accumulate in the reactive mixture. Indeed, sonication for 1h yielded an aqueous phase with up to ~88 mM (confirmed via electrochemical, colorimetric, and vibrational spectroscopy[30] methods, Figures S3, S4 and S6). These experiments highlight the simplicity of the SEWM approach in producing H_2O_2 at higher concentrations.

The observation that dissolved O_2 redox produces H_2O_2 prompts the question about the origin of OH• in SEWMs. To explore the origin of these ROS, we ultrasonicated a 1:1 mixture of 100 mM aqueous 3,4-dihydro-2,3-dimethyl-2H-pyrrole 1-oxide (DMPO) and hexadecane oil for 30 minutes, under ambient and deaerated solutions. DMPO was used as a spin trap to capture and stabilize any formed radicals to be detected through ESR spectroscopy of the water phase (Supplementary Note S5) (**Figure 2A**).[31, 32] The ESR spectra of the sonicated water phase from a glass container under ambient conditions (**Figure 2B**) exhibited distinct paramagnetic splitting features with a 1:2:2:1 integration ratio and hyperfine coupling constants of α^N = 14.9 G and α_β^H = 14.88 G, confirming the formation of [DMPO−OH] adducts and the production of OH•. Spectral deconvolution also revealed a weak signal with 1:1:1 integration ratio which may originate from the dimerization of DMPO-OH (α^N = 14.45 G), seen as triplet in which no α^N is observed due to the absence of hydrogen at the β-position of DMPO in the dimer.[33] Importantly, the deconvolution also revealed an oxygen-centered radical trapped by DMPO. The [DMPO−OR] species (where R represents an alkyl radical) exhibited a 1:1:1:1:1:1 profile, with hyperfine coupling constants of αN = 14.58 G and α_β^H = 11.08 G, closely matching the reported values for DMPO−OR species (α^N = 14.51 G and α_β^H = 10.71 G).[32] A similar sextuplet pattern has also been ascribed to a DMPO-R species in a microdroplet experiment.[21] Such radicals could result from the degradation of hexadecane.[27] To further validate this, the NMR of the sonicated hexadecane oil showed the formation of an alcohol (likely hexadecanol), as probed by both 1H and 13C NMR (Figure S10). Overall, these experiments suggest that O_2 reduction to H_2O_2 is likely facilitated by reducing intermediates (H•) or electron transfer reactions mediated through oil oxidation in the emulsion.

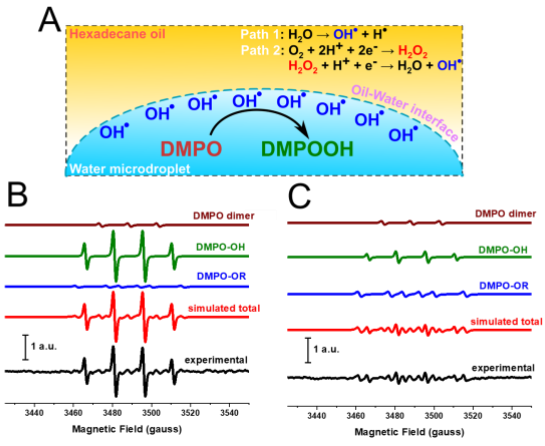

Figure 2: ESR analysis of the sonicated water phase to investigate the source of OH• radicals. (A) Schematic illustrating the interaction between OH• radicals and DMPO as a spin trap. (B) ESR spectra of the sonicated water phase with DMPO under ambient conditions and (C) argon conditions.

Furthermore, a similar ESR profile for an SEWMs performed in a plastic container (Figure S9A) instead of glass suggests that vial material has minimal impact on OH• generation, thus emphasizing the catalyst-free nature of these experiments. Interestingly, the ESR spectra of ultrasonicated 100 mM aqueous DMPO without hexadecane oil did not exhibit any paramagnetic signals (Figure S9), confirming that no radicals were generated. Based on these observations, it can be inferred that the liquid biphasic nature of the SEWMs created by the hydrophobic hexadecane oil is critical to form OH• radicals and to enable redox, creating pathways that are distinct to those known for the sonochemistry of single phases.[34]

We now turn to the exploration of OH• radical formation in SEWMs in the absence of oxygen. In this case, the resulting ESR spectra from the sonicated water phase (**Figure 2C**) also displayed a splitting feature with a 1:2:2:1 integration ratio, indicating OH• formation. However, the signal intensity was one order of magnitude smaller than that under ambient conditions. This aligns with the minimal H_2O_2 detection under argon-saturated conditions, confirming that O_2 reduction significantly contributes to OH• formation. Given that H_2O_2 is generally believed to form from the dimerization of two OH• radicals (**reaction 2)**, we also tested the possibility of supressing its formation by adding excess DMPO (250 mM) to a mixture of water and hexadecane oil (1:10 volume ratio). If H_2O_2 is primarily formed from the combination of OH• radicals, its concentration is expected to decrease due to DMPO scavenging the generated radicals. Because the DMPO-OH adduct is redox active,[31] colorimetric H_2O_2 tests were conducted (Figure S11), showing similar concentrations of peroxide in mixtures with and without DMPO. This suggests that H_2O_2 likely forms through O_2 reduction rather than radical combination. These experiments helped confirm that O_2 is the source of both H_2O_2 and OH•, possibly as a result of **reaction 7** or the reverse of **reaction 2** where homolysis of H_2O_2 could be caused by sonication.

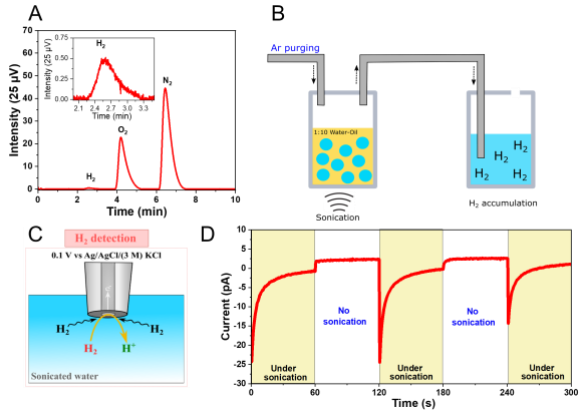

Figure 3: Detection and quantification of H_2 generated by SEWMs. (A) GC–TCD chromatograms illustrating H_2 production during sonication of hexadecane and water. Injection sample volume was 300 µL and Ar was used as the carrier gas. Baseline correction was applied before plotting, and peaks corresponding to H_2, O_2, and N_2 are labeled. The inset zooms in on the H_2 peak, the integrated area of which corresponds to 1.5 nmol of H_2 in 300 µL (see Fig. S12 in the SI). (B) Schematic illustrating the setup for H_2 detection using a headspace approach. (C) Schematic of the experimental setup for H_2 detection in the sonicated water phase, using a 12.5 µm Pt-UME biased at 0.1 V vs. Ag/AgCl (3M KCl). (D) Chronoamperograms recorded during sonication with a 12.5 µm Pt-UME biased at 0.1 V vs. Ag/AgCl (3M KCl).

Finally, we tested the reducing power of the species generated by the SEWMs. First, we detected H_2 using a headspace approach with gas chromatography equipped with a thermal conductivity detector (GC–TCD). **Figure 3A** shows the recorded chromatograms, confirming formation of H_2 with a concentration of 5 nmol per mL of headspace after sonication of a 1:10 mixture of water and hexadecane oil for 15 min. Additionally, we demonstrated H_2 formation using a simple, qualitative, and affordable electrochemical approach adaptable for H_2 detection, as illustrated in **Figure 3B**. In this setup, a 1:10 mixture of water and hexadecane oil was sonicated in one vial, while the headspace gases were directed into a second vial serving as both a collector and an electrochemical cell. A Pt-UME was used as the H_2 amperometric detector (**Figure S2A**), held at 0.1 V vs. Ag/AgCl/3 M KCl to facilitate H_2 oxidation, as depicted in Figure 3C.[28] During sonication, a distinct anodic current was recorded at the Pt-UME, indicating H_2 formation by SEWMs (**Figure 3D**). In contrast, when sonication was stopped, only a background cathodic current was observed, likely due to O_2 reduction at the Pt-UME. H_2 could be generated within SEWMs via mechanisms involving the formation of H• from hexadecane oil degradation (radical mediation, **Reaction** 8) or via the hydrogen evolution reaction (electron transfer mediation, **Reaction 9**) involving protons in the aqueous solution. Further studies are required to ascertain the origin of H_2, but our results conclusively show its generation.

$$H^{\bullet} + H^{\bullet} \rightleftharpoons H_2 \qquad \text{Reaction 8}$$

$$2H^+ + 2e^- \rightleftharpoons H_2 \qquad \text{Reaction 9}$$

We further tested the ability of SEWMs to perform electroless deposition on a metal substrate. Herein, we ultrasonicated a 1:10 mixture of 1 mM aqueous $Pb(NO_3)_2$ and hexadecane in the presence of an Au wire (50 µm diameter, 1 cm length) inserted in the sonicated container. We then performed ex-situ SEM/EDX to characterize the changes on the Au surface (**Figure 4A,** Supplementary note S8). It is evident from these images that islands of Pb have been deposited on the Au wire. This observation underscores that Pb^{2+} ions, with a standard reduction potential of -0.126 V vs. SHE, are reduced in SEWMs during sonication (**Figure 4B**) without any external potential. A similar behaviour was also observed on a Cu metal surface (Figure S13). This reducing power is certainly sufficient to produce H_2 and to reduce O_2 to H_2O_2 (**reaction 6** with formal reduction potential ~0.29 V vs. SHE at pH 7), thus validating our results. These findings, combined with the ESR and electrochemical measurements, underscore the ability of the microdroplets to function as redox microreactors.

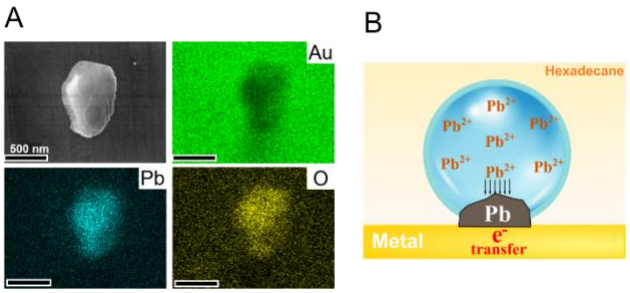

Figure 4: Electroless deposition of Pb^{2+} SEWMs. (A) SEM and EDX images of Pb deposited on a 50 µm Au wire via SEWMs. (B) Schematic illustrating the collision mechanism involved in the electroless deposition of Pb^{2+} on Au using SEWMs.

In this communication, we established the reductive character of SEWMs and identified the origin of key redox and chemical intermediates using (electro)chemical analysis and electron spin resonance. In contrast to the view that oxidative chemistry drives the production of $OH^{\bullet}$ and H_2O_2, we demonstrate that it is the reduction of dissolved O_2 which controls their generation, facilitated by the reducing power of SEWMs. This was further confirmed by the increased formation of H_2O_2 (accumulated up to ~88 mM in the aqueous phase) by simply procuring a constant supply of O_2 in SEWMs. Furthermore, the reducing power of the SEWMs was validated through the detection of H_2 and the electroless deposition of Pb^{2+} onto a metal surface. While our findings suggest the reduction of O_2 to H_2O_2, the generation of H_2, and metal electrodeposition within SEWMs, the precise mechanism underlying the generation of this reducing power, including the potential involvement of radicals and/or electrons is yet to be elucidated.

SEWMs operate catalyst-free and without the need for an external voltage source, but the redox mechanistic insight gained here opens new opportunities at improving their performance for the 2e ORR and other reactions, using concepts of electrocatalysis which may not seem evident at first.[35, 36] Distinct to the sole contributions of sonochemistry or emulsion electrochemistry,[34, 37] our group is currently engaged in enhancing the reactivity, selectivity, and yields of (electro)chemical reactions using SEWMs as unique, catalyst-free redox microreactors.

ASSOCIATED CONTENT

Additional experimental details, materials and methods used; preparation of microdroplet emulsion (Supplementary note S1); electrochemical detection of H_2 and H_2O_2(Supplementary note S2); Iodometric detection of H_2O_2 (Supplementary note S3); Mass Spectrometry measurements (Supplementary note S4); Electron Spin Resonance (ESR) spectroscopy (Supplementary note S5); Nuclear Magnetic Resonance (NMR) measurements (Supplementary note S6); Gas chromatography (GC) thermal conductivity detector (TCD) analysis (Supplementary note S7); SEM and EDX of Pb electrodeposited on Au and Cu substrates (Supplementary note S8). This material is available free of charge via the Internet at http://pubs.acs.org.

AUTHOR INFORMATION

Corresponding Author

* Joaquín Rodríguez-López - Department of Chemistry, University of Illinois Urbana-Champaign, Urbana, IL 61801, USA.

Author Contributions

‡ Authors A. Asserghine and A. Baby contributed equally.

ACKNOWLEDGMENT

This material is based upon work supported by the U.S. Department of Energy, Office of Science, Science Foundations for Energy Earthshots Program, under Award Number DE-SC0024892. The authors express their gratitude to Hung Nguyen from Charles M. Schroeder's group for assistance in generating the microdroplet image and to Dr. Haijun Yao for his invaluable guidance and support with mass spectrometry analysis. Disclaimer: "This report was prepared as an account of work sponsored by an agency of the United States Government. Neither the United States Government nor any agency thereof, nor any of their employees, makes any warranty, express or implied, or assumes any legal liability or responsibility for the accuracy, completeness, or usefulness of any information, apparatus, product, or process disclosed, or represents that its use would not infringe privately owned rights. Reference herein to any specific commercial product, process, or service by trade name, trademark, manufacturer, or otherwise does not necessarily constitute or imply its endorsement, recommendation, or favoring by the United States Government or any agency thereof. The views and opinions of authors expressed herein do not necessarily state or reflect those of the United States Government or any agency thereof.

REFERENCES

(1) Lee, J. K.; Samanta, D.; Nam, H. G.; Zare, R. N. Micrometer-Sized Water Droplets Induce Spontaneous Reduction. *J. Am. Chem. Soc.* **2019**, *141* (27), 10585–10589. DOI: 10.1021/jacs.9b03227

(2) Qiu, L.; Cooks, R. G. Simultaneous and Spontaneous Oxidation and Reduction in Microdroplets by the Water Radical Cation/Anion Pair. *Angew. Chem*. **2022**, *134* (41), e202210765. DOI: 10.1002/ange.202210765

(3) Jung, Y.; Marcus, R. A. On the Theory of Organic Catalysis "On Water." *J. Am. Chem. Soc*. **2007**, *129* (17), 5492–5502. DOI: 10.1021/ja068120f

(4) Banerjee, S.; Zare, R. N. Syntheses of Isoquinoline and Substituted Quinolines in Charged Microdroplets. *Angew. Chem*. **2015**, *127* (49), 15008–15012. DOI: 10.1002/anie.201507805.

(5) Bain, R. M.; Pulliam, C. J.; Cooks, R. G. Accelerated Hantzsch Electrospray Synthesis with Temporal Control of Reaction Intermediates. *Chem. Sci*. **2015**, *6* (1), 397–401. DOI: 10.1039/C4SC02436B

(6) Yan, X.; Cheng, H.; Zare, R. N. Two-Phase Reactions in Microdroplets without the Use of Phase-Transfer Catalysts. *Angew. Chem*. **2017**, *129* (13), 3616–3619. DOI: 10.1002/ange.201612308

(7) Meng, Y.; Gnanamani, E.; Zare, R. N. One-Step Formation of Pharmaceuticals Having a Phenylacetic Acid Core Using Water Microdroplets. *J. Am. Chem. Soc.* **2023**, *145* (14), 7724–7728. DOI: 10.1021/jacs.3c00773

(8) Li, J.; Liu, C.; Chen, H.; Zare, R. N. Accelerated Oxidation of Organic Sulfides by Microdroplet Chemistry. *J. Org. Chem.* **2021**, *86* (7), 5011–5015. DOI: J. Org. Chem. 2021, 86 (7), 5011–5015.

(9) Song, X.; Basheer, C.; Zare, R. N. Making Ammonia from Nitrogen and Water Microdroplets. *Proc. Natl. Acad. Sci.*

U.S.A. **2023**, *120* (16), e2301206120. DOI: 10.1073/pnas.2301206120

(10) Kumar, A.; Mondal, S.; Mofidfar, M.; Zare, R. N.; Banerjee, S. Capturing Reactive Carbanions by Microdroplets. *J. Am. Chem. Soc.* **2022**, *144* (17), 7573–7577. DOI: 10.1021/jacs.2c01577

(11) Mehrgardi, M. A.; Mofidfar, M.; Zare, R. N. Sprayed Water Microdroplets Are Able to Generate Hydrogen Peroxide Spontaneously. *J. Am. Chem. Soc.* **2022**, *144* (17), 7606–7609. DOI: 10.1021/jacs.2c02890

(12) Rao, Z.; Li, X.; Fang, Y.-G.; Francisco, J. S.; Zhu, C.; Chu, C. Spontaneous Oxidation of Thiols and Thioether at the Air–Water Interface of a Sea Spray Microdroplet. *J. Am. Chem. Soc.* **2023**, *145* (19), 10839–10846. DOI: 10.1021/jacs.3c02334

(13) Ai, Y.; Xu, J.; Gunawardena, H. P.; Zare, R. N.; Chen, H. Investigation of Tryptic Protein Digestion in Microdroplets and in Bulk Solution. *J. Am. Soc. Mass Spectrom.* **2022**, *33* (7), 1238–1249. DOI: 10.1021/jasms.2c00072

(14) Vannoy, K. J.; Dick, J. E. Oxidation of Cysteine by Electrogenerated Hexacyanoferrate (III) in Microliter Droplets. *Langmuir* **2022**, *38* (39), 11892–11898. DOI: 10.1021/acs.langmuir.2c01385

(15) Lee, K.; Lee, H.-R.; Kim, Y. H.; Park, J.; Cho, S.; Li, S.; Seo, M.; Choi, S. Q. Microdroplet-Mediated Radical Polymerization. *ACS Cent. Sci.* **2022**, *8* (9), 1265–1271. DOI: 10.1021/acscentsci.2c00694

(16) Lee, K.; Cho, Y.; Kim, J. C.; Choi, C.; Kim, J.; Lee, J. K.; Li, S.; Kwak, S. K.; Choi, S. Q. Catalyst-Free Selective Oxidation of C(sp3)-H Bonds in Toluene on Water. *Nat. Commun*. **2024**, *15* (1), 6127. DOI: 10.1038/s41467-024-50352-7

(17) Yuan, G.; Jin, Z.; Cao, Y.; Schulz, H.-M.; Gluyas, J.; Liu, K.; He, X.; Wang, Y. Microdroplets Initiate Organic-Inorganic Interactions and Mass Transfer in Thermal Hydrous Geosystems. *Nat. Commun*. **2024**, *15* (1), 4960. DOI: 10.1038/s41467-024-49293-y

(18) Yuan, X.; Zhang, D.; Liang, C.; Zhang, X. Spontaneous Reduction of Transition Metal Ions by One Electron in Water Microdroplets and the Atmospheric Implications. *J. Am. Chem. Soc.* **2023**, *145* (5), 2800-2805. DOI: 10.1021/jacs.3c00037

(19) Xiong, H.; Lee, J. K.; Zare, R. N.; Min, W. Strong Electric Field Observed at the Interface of Aqueous Microdroplets. J. Phys. Chem. Lett. **2020**, *11* (17), 7423–7428. DOI: 10.1021/acs.jpclett.0c02061

(20) Heindel, J. P.; LaCour, R. A.; Head-Gordon, T. The Role of Charge in Microdroplet Redox Chemistry. *Nat. Commun.* **2024**, *15* (1), 3670. DOI: 10.1038/s41467-024-47879-0

(21) Chen, X.; Xia, Y.; Wu, Y.; Xu, Y.; Jia, X.; Zare, R. N.; Wang, F. Sprayed Oil–Water Microdroplets as a Hydrogen Source. *J. Am. Chem. Soc.* **2024**, *146* (15), 10868–10874. DOI: 10.1021/jacs.4c01455

(22) Eatoo, M. A.; Mishra, H. Busting the Myth of Spontaneous Formation of H_2O_2 at the Air–Water Interface: Contributions of the Liquid–Solid Interface and Dissolved Oxygen Exposed. Chem. Sci. **2024**, 15 (9), 3093–3103. DOI: 10.1039/D3SC06534K.

(23) Gallo Jr, A.; Musskopf, N. H.; Liu, X.; Yang, Z.; Petry, J.; Zhang, P.; Thoroddsen, S.; Im, H.; Mishra, H. On the Formation of Hydrogen Peroxide in Water Microdroplets. *Chem. Sci.* **2022**, *13* (9), 2574–2583. DOI: 10.1039/D1SC06465G

(24) Li, K.; Ge, Q.; Liu, Y.; Wang, L.; Gong, K.; Liu, J.; Xie, L.; Wang, W.; Ruan, X.; Zhang, L. Highly Efficient Photocatalytic H2O2 Production in Microdroplets: Accelerated Charge Separation and Transfer at Interfaces. *Energy Environ. Sci.* **2023**, *16* (3), 1135–1145. DOI: 10.1039/D2EE03774B

(25) Qiu, L.; Cooks, R. G. Spontaneous Oxidation in Aqueous Microdroplets: Water Radical Cation as Primary Oxidizing Agent. *Angew. Chem.* **2024**, *136* (17), e202400118. DOI: 10.1002/ange.202400118

(26) Shi, X.; Siahrostami, S.; Li, G.-L.; Zhang, Y.; Chakthranont, P.; Studt, F.; Jaramillo, T. F.; Zheng, X.; Nørskov, J. K. Understanding Activity Trends in Electrochemical Water Oxidation to Form Hydrogen Peroxide. *Nat. Commun.* **2017**, *8* (1), 701. DOI: 10.1038/s41467-017-00585-6

(27) Ganguly, M.; Debraj, D.; Mazumder, N.; Carpenter, J.; Manickam, S.; Pandit, A. B. Impact of Ultrasonication on the Oxidative Stability of Oil-in-Water Nanoemulsions: Investigations into Kinetics and Strategies to Control Lipid Oxidation. *Ind. Eng. Chem. Res.* **2024**, *63* (23) 10212–10225. DOI: 10.1021/acs.iecr.4c00506

(28) Asserghine, A.; Baby, A.; Putnam, S. T.; Qian, P.; Gao, E.; Zhao, H.; Rodríguez-López, J. In Situ Detection of Reactive Oxygen Species Spontaneously Generated on Lead Acid Battery Anodes: A Pathway for Degradation and Self-Discharge at Open Circuit. *Chem. Sci.* **2023**, *14* (43), 12292–12298. DOI: 10.1039/D3SC04736A

(29) Berbille, A.; Li, X.-F.; Su, Y.; Li, S.; Zhao, X.; Zhu, L.; Wang, Z. L. Mechanism for Generating H_2O_2 at Water–Solid Interface by Contact Electrification. *Adv. Mater.* **2023**, *35* (46), 2304387. DOI: 10.1002/adma.202304387

(30) Cao, P.; Xie, Q.; Nie, X.; Zhao, K.; Liu, Y.; Chen, S.; Yu, H.; Chen, J. G. Metal Single-Site Catalyst Design for Electrocatalytic Production of Hydrogen Peroxide at Industrial-Relevant Currents. *Nat. Commun.* **2023**, *14* (1), 172. DOI: 10.1038/s41467-023-35839-z

(31) Barroso-Martínez, J. S.; Romo, A. I. B.; Pudar, S.; Putnam, S. T.; Bustos, E.; Rodríguez-López, J. Real-Time Detection of Hydroxyl Radical Generated at Operating Electrodes via Redox-Active Adduct Formation Using Scanning Electrochemical Microscopy. *J. Am. Chem. Soc*. **2022**, *144* (41), 18896–18907. DOI: 10.1021/jacs.2c06278

(32) Guo, Q.; Qian, S. Y.; Mason, R. P. Separation and Identification of DMPO Adducts of Oxygen-Centered Radicals Formed from Organic Hydroperoxides by HPLC-ESR, ESI-MS, and MS/MS. J. Am. Soc. Mass Spectrom. **2003**, 14 (8), 862–871. DOI: 10.1016/S1044-0305(03)00336-2.

(33) Fontmorin, J. M.; Burgos Castillo, R. C.; Tang, W. Z.; Sillanpää, M. Stability of 5,5-Dimethyl-1-Pyrroline-N-Oxide as a Spin-Trap for Quantification of Hydroxyl Radicals in Processes Based on Fenton Reaction. Water Res. 2016, 99, 24–32. DOI: 10.1016/j.watres.2016.04.053.

(34) Suslick, K. S. Sonochemistry. *Science* **1990**, *247* (4949), 1439–1445. DOI: 10.1126/science.247.4949.1439

(35) Adams, J. S.; Kromer, M. L.; Rodríguez-López, J.; Flaherty, D. W. Unifying Concepts in Electro- and Thermocatalysis Toward Hydrogen Peroxide Production. J. Am. Chem. Soc. 2021, 143 (21), 7940–7957. DOI: 10.1021/jacs.0c13399

(36) Zhao, Y.; Adams, J.S.; Baby, A.; Kromer, M.L.; Flaherty, D.W.; Rodríguez-López, J. Electrochemical Screening of Au/Pt Catalysts for the Thermocatalytic Synthesis of Hydrogen Peroxide Based on Their Oxygen Reduction and Hydrogen Oxidation Activities Probed via Voltammetric Scanning Electrochemical Microscopy. *ACS Sustainable Chem. Eng*.

2022, *10* (51) 17207–17220. DOI: 10.1021/acssuschemeng.2c05120

(37) Santiago-Carboney, A.; Konstantinov, F.; Pence, M. A.; Barth, B. A.; Imel, A.; Zawodzinski, T.; Rodríguez-López, J. Correlation Between Microscopic Current Fluctuations Observed at Ultra-Microelectrodes and Macroscopic Bulk Electrolysis Performance in Redox-Active Microemulsions. *J. Electrochem. Soc.* **2024**, *171* (11), 110502. DOI: 10.1149/1945-7111/ad8bf7

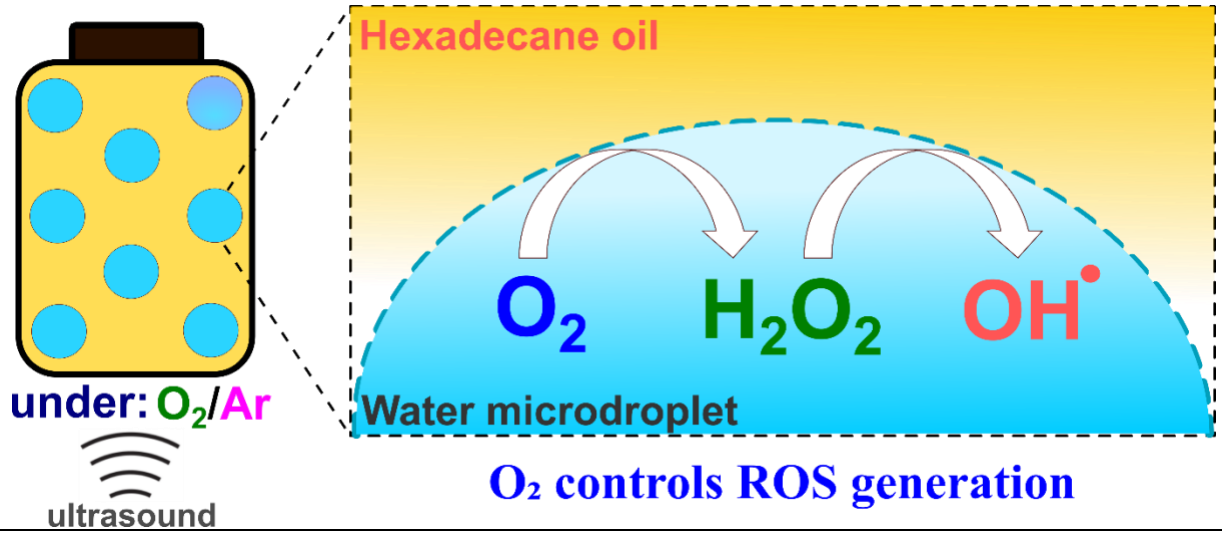

O_2 controls ROS generation